

Pushing the boundaries
of chemistry?
It takes
#HumanChemistry

Make your curiosity and talent as a chemist matter to the world with a specialty chemicals leader. Together, we combine cutting-edge science with engineering expertise to create solutions that answer real-world problems. Find out how our approach to technology creates more opportunities for growth, and see what chemistry can do for you at:

[evonik.com/career](https://www.evonik.com/career)



Selective Effects of the Host Matrix in Hydrogenated InGaAsN Alloys: Toward an Integrated Matrix/Defect Engineering Paradigm

Francesco Filippone,* Saeed Younis, Giuseppe Mattioli, Marco Felici, Elena Blundo, Antonio Polimeni, Giorgio Pettinari, Damiano Giubertoni, Eduard Sterzer, Kerstin Volz, Dan Fekete, Eli Kapon, and Aldo Amore Bonapasta

Saeed Younis, one of our co-authors, prematurely passed away while this manuscript was being prepared. This work is dedicated to him

In dilute nitride $\text{In}_y\text{Ga}_{1-y}\text{As}_{1-x}\text{N}_x$ alloys, a spatially controlled tuning of the energy gap can be realized by combining the introduction of N atoms—inducing a significant reduction of this parameter—with that of hydrogen atoms, which neutralize the effect of N. In these alloys, hydrogen forms N–H complexes in both Ga-rich and In-rich N environments. Here, photoluminescence measurements and thermal annealing treatments show that, surprisingly, N neutralization by H is significantly inhibited when the number of In–N bonds increases. Density functional theory calculations account for this result and reveal an original, physical phenomenon: only in the In-rich N environment, the $\text{In}_y\text{Ga}_{1-y}\text{As}$ host matrix exerts a selective action on the N–H complexes by hindering the formation of the complexes more effective in the N passivation. This thoroughly overturns the usual perspective of defect-engineering by proposing a novel paradigm where a major role pertains to the defect-surrounding matrix.

1. Introduction

Previous studies of hydrogenated dilute-nitride III–V–N alloys focused on two phenomena having remarkable effects on the band gap energy: a significant decrease of the III–V alloy band gap induced by small percentages of N and the partial or full recovery of the N-free alloy band gap induced by atomic hydrogen incorporation.^[1–3] Those studies clarified also the central role of the N–H complexes in the N neutralization.^[1,4–8] In $\text{GaAs}_{1-x}\text{N}_x$, H fully neutralizes the effects of N. This phenomenon was exploited for the realization of single-photon emitters using a spatially selective hydrogen incorporation/removal at the sub-micrometer scale, which


F. Filippone, G. Mattioli, A. Amore Bonapasta
ISM-CNR

Istituto di Struttura della Materia –Consiglio Nazionale delle Ricerche
Via Salaria Km 29.5, Monterotondo I-00015, Italy
E-mail: francesco.filippone@cnr.it

S. Younis, M. Felici, E. Blundo, A. Polimeni
Dipartimento di Fisica and CNISM
Sapienza Università di Roma
Piazzale A. Moro 2, Roma I-00185, Italy

G. Pettinari
CNR-IFN

Istituto di Fotonica e Nanotecnologie–Consiglio Nazionale delle Ricerche
Via Cineto Romano, 42, Rome I-00156, Italy

 The ORCID identification number(s) for the author(s) of this article can be found under <https://doi.org/10.1002/adfm.202108862>.

© 2021 The Authors. Advanced Functional Materials published by Wiley-VCH GmbH. This is an open access article under the terms of the Creative Commons Attribution-NonCommercial License, which permits use, distribution and reproduction in any medium, provided the original work is properly cited and is not used for commercial purposes.

DOI: 10.1002/adfm.202108862

D. Giubertoni
Sensors and Devices
Fondazione Bruno Kessler
Centre for Materials and Microsystems
Micro Nano Facility
Via Sommarive 18, Trento 38123, Italy

E. Sterzer, K. Volz
Department of Physics and Material Sciences Center
Philipps University Marburg
Marburg 35032, Germany

D. Fekete, E. Kapon
Ecole Polytechnique Fédérale de Lausanne (EPFL)
Laboratory of Physics of Nanostructures
Lausanne CH-1015, Switzerland

D. Fekete
Department of Physics
Technion-Israel Institute of Technology
Haifa 32000, Israel

permitted a spatial tuning of the energy gap.^[9–11] This approach would be even more interesting in $\text{In}_y\text{Ga}_{1-y}\text{As}_{1-x}\text{N}_x$, whose band gap energy may be brought in the telecommunication wavelength range.^[12] However, indications of an uncertain N passivation in hydrogenated $\text{InAs}_{1-x}\text{N}_x$ ^[13–15] have prompted the need to understand the conditions that may favor or not such passivation in $\text{In}_y\text{Ga}_{1-y}\text{As}_{1-x}\text{N}_x$ alloys, where the local N environment ranges from 4Ga-N clusters (encountered in GaAsN) to 4In-N clusters (as it occurs in InAsN). Such an issue has motivated the present study, focused on possible relationships between the cationic environment of N atoms and a different H efficiency in the neutralization of the effects of N. These relationships have been investigated here by combining annealing treatments with photoluminescence (PL) spectroscopy measurements. In this regard, previous studies showed that, in InGaAsN, thermal annealing increases both the number of In-N bonds and the band gap energy.^[16–18] Therefore, PL measurements combined with annealing treatments provide a quite reliable method to ascertain the migration of In atoms toward N as well as how the variation of the N environment from a Ga-rich to an In-rich one can affect hydrogen's ability to neutralize the effects of N. Present PL investigations of $\text{In}_y\text{Ga}_{1-y}\text{As}_{1-x}\text{N}_x$ quantum wells (QWs) show that, for increasing H doses, the alloy band gap energy increases, but it does not reach the corresponding N-free $\text{In}_y\text{Ga}_{1-y}\text{As}$ band gap energy. Moreover, the measurement of the dependence of the band gap recovery of hydrogenated InGaAsN on the thermal annealing temperature shows that an In-rich environment for N atoms results in a much lower degree of N passivation. At first glance, this result seems explained by the occurrence of an N environment in the annealed InGaAsN alloy similar to that present in InAsN, which would induce a similar hydrogen behavior. Instead, present Density Functional Theory (DFT) investigations reveal a thoroughly novel phenomenon, fully explaining the experimental findings: in InGaAsN,

only in the case of the In-rich N environment, the host InGaAs matrix exerts a selective action on the N–H complexes, by hindering the formation of the most efficient complexes for the N passivation. The increase of In-N clusters is accompanied therefore by a decrease in the number of the most effective N–H complexes and, then, by a reduced neutralization of the N effects. This previously unknown host-matrix effect can induce an evolution from the usual material design protocols toward integrated matrix/defect engineering approaches.

2. Results and Discussion

2.1. Experimental Results

A double QW InGaAsN/InGaAs sample was exposed to a hydrogen ion beam, as sketched in **Figure 1a**. **Figure 1b** shows the room temperature PL spectra of the pristine and hydrogenated samples for increasing H dose, d_H . We readily notice that the energy of the emission peak of the N-free reference is unchanged with d_H . Instead, a sizable blue-shift of the PL peak of the N-containing QW is observed, indicating N passivation by H. This, in turn, leads to a band gap increase of the InGaAsN material toward the band gap of the N-free host lattice. However, above a given H dose the band gap opening is halted and further H treatments do not cause sizable changes in the PL spectra, see topmost curve in **Figure 1b**. This is clearly very different with respect to In-free GaAsN, where a full passivation of the N atoms can be achieved.^[8]

The most simple and straightforward explanation of the behavior described in **Figure 1b** could be related to a different In content in the two QWs; however, secondary ion mass spectrometry (SIMS) measurements rule out such an hypothesis, see **Figure 1c**.

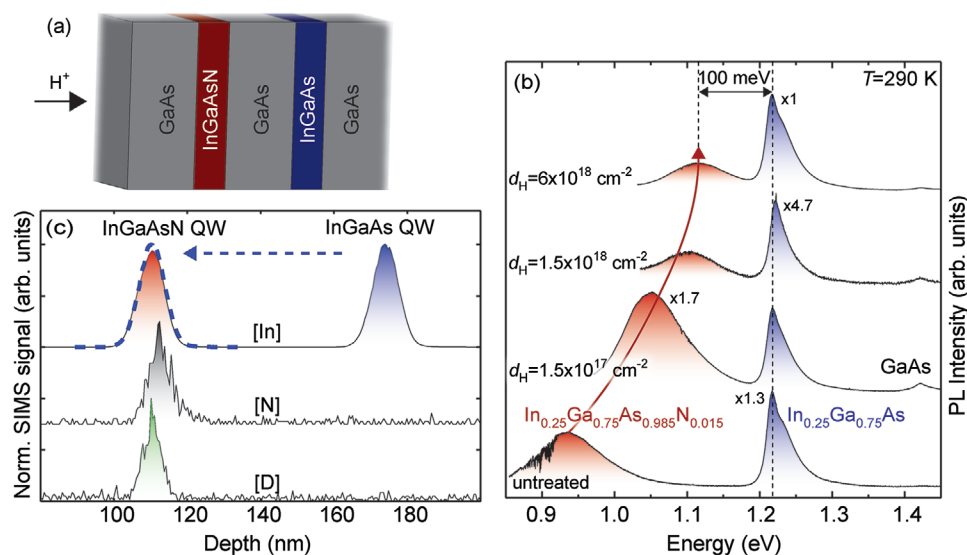


Figure 1. a) Sketch of the sample structure. The sample contains an $\text{In}_{0.25}\text{Ga}_{0.75}\text{As}_{0.985}\text{N}_{0.015}$ QW and a reference $\text{In}_{0.25}\text{Ga}_{0.75}\text{As}$ QW, which have an equal thickness of 5.6 nm and are separated by a 50 nm-thick GaAs barrier. b) Room temperature photoluminescence (PL) spectra of the double QW for different H doses, d_H . The PL peaks corresponding to the N-containing and N-free QWs are indicated. c) SIMS depth profile of the deuterated double QW sample. The depth profile of each atomic species is indicated in the figure. The $\text{In}_{0.25}\text{Ga}_{0.75}\text{As}$ In peak has been projected onto the $\text{In}_{0.25}\text{Ga}_{0.75}\text{As}_{0.985}\text{N}_{0.015}$ one, as shown by the dashed line, to highlight the very similar In concentrations and thicknesses in the two QWs.

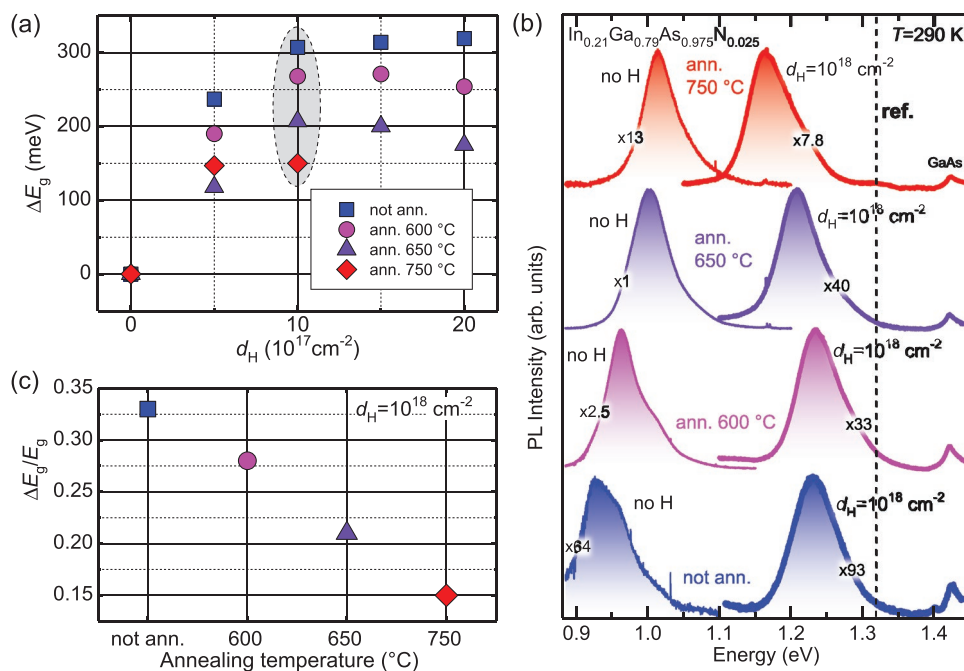


Figure 2. a) Blue-shift of the PL peak energy (ΔE_g) induced by different H doses (d_H) in the $\text{In}_{0.21}\text{Ga}_{0.79}\text{As}_{0.975}\text{N}_{0.025}$ QW annealed at 600, 650, and 750 °C, (for 10, 30, and 10 s, respectively), as well as in a nonannealed sample. Notice the saturation of the peak energy for $d_H = 10^{18} \text{ cm}^{-2}$. b) Room temperature photoluminescence spectra of the $\text{In}_{0.21}\text{Ga}_{0.79}\text{As}_{0.975}\text{N}_{0.025}$ QW for different post-growth annealings (including the not annealed sample, bottom-most spectra) and hydrogenation with a H dose d_H of 10^{18} cm^{-2} . For each annealing, the spectra of the not hydrogenated and of the hydrogenated sample are shown. The vertical dashed line labeled as ref. indicates the QW emission energy of an $\text{In}_{0.21}\text{Ga}_{0.79}\text{As}$ QW. The energy was calculated within the envelope function approximation using the nominal QW parameters. c) $\Delta E_g/E_g$ ratio measured for the same QW of Panel (b) at different annealing temperatures.

The results presented so far indicate that H is significantly less effective at passivating N atoms in In-containing dilute nitrides with respect to the GaAsN case. We will show that this finding is related to the local N environment. Thus, we further investigated this issue by performing a series of thermal annealing treatments on InGaAsN single QWs, which are known to favor the formation of 4In-N clusters in this material.^[17]

Figure 2a shows the blue-shift of the PL peak energy (ΔE_g) induced by different H doses (d_H) in samples containing an $\text{In}_{0.21}\text{Ga}_{0.79}\text{As}_{0.975}\text{N}_{0.025}$ QW annealed at 600, 650, and 750 °C, as well as not subjected to any thermal treatment. The shift of the PL peak energy saturates at $d_H = 10^{18} \text{ cm}^{-2}$, where the maximum band gap recovery is attained for all the investigated samples.

The PL spectra of the three annealed samples irradiated with this H dose are shown in Figure 2b. The bottom-most spectra refer to a nonannealed sample before and after H irradiation. The hydrogenated, not annealed QW shows a blue-shift of the PL peak energy of about $\Delta E_g = 300 \text{ meV}$. In the annealed samples—thus characterized by an In-rich environment around the N atoms^[16–18]—two different behaviors can be observed. First, in the H-free QWs, the PL peak moves at higher energy with increasing annealing temperature, in agreement with the mentioned, previous studies.^[16,17] Second, the amount of band gap recovery induced by hydrogenation decreases rapidly with increasing annealing temperature. This latter finding indicates that an In-rich neighborhood inhibits the N atom passivation.

Table 1 and Figure 2c summarize these experimental results. In particular, they report the variation of the $\Delta E_g/E_g$ ratio for different annealing conditions. This quantity depends strongly

on the annealing temperature, further strengthening the indication given by the E_g trend in Table 1.

2.2. Theoretical Results

N–H complexes in the $\text{In}_{0.21}\text{Ga}_{0.79}\text{As}_{0.975}\text{N}_{0.025}$ alloy were investigated by applying two simplifying assumptions: i) 4Ga-N and 4In-N clusters were considered as representatives of Ga-rich and In-rich N environments, respectively, by disregarding clusters of intermediate composition, and ii) the as-grown and thermally annealed samples of the same alloy were simulated by two “extreme” models, characterized by the presence of 4Ga-N clusters only and 4In-N clusters only, respectively, in an ideal $\text{In}_{0.20}\text{Ga}_{0.80}\text{As}_{0.97}\text{N}_{0.03}$ alloy (details in Section S1, Supporting Information).

Table 1. The first row of the Table reports the band gap energies, E_g , estimated by the PL spectra of Figure 2b for the as grown and annealed $\text{In}_{0.21}\text{Ga}_{0.79}\text{As}_{0.975}\text{N}_{0.025}$ QWs before hydrogenation. The corresponding E_g values after hydrogenation, differences between the latter and the former E_g values, ΔE_g , and $\Delta E_g/E_g$ ratios are reported in the second, third, and fourth row, respectively.

	AG (as grown)	ANN (600 °C)	ANN (650 °C)	ANN (750 °C)
E_g (InGaAsN) [eV]	0.930	0.962	1.002	1.016
E_g (InGaAsN + H) [eV]	1.231	1.234	1.210	1.163
ΔE_g [eV]	0.301	0.272	0.208	0.147
$\Delta E_g/E_g$	32%	28%	21%	14%

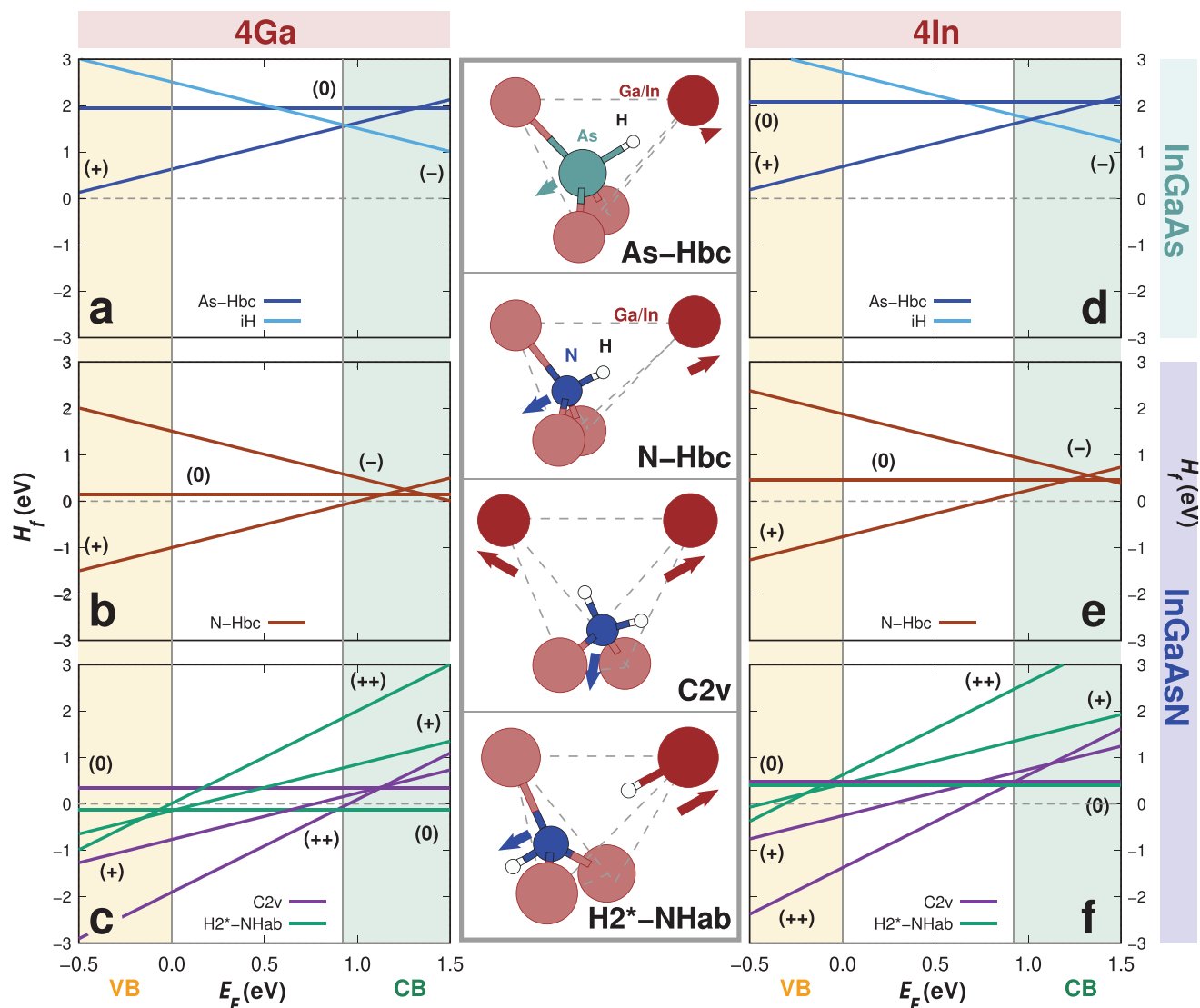


Figure 3. The geometries of the most important As-H and N-H complexes investigated here are shown in the central panel of the figure. The arrows highlight the displacements of the atoms in the complex from their unrelaxed position. The dashed lines draw a tetrahedron formed by the four Ga or In atoms neighboring the N atom involved in the complex. The three topmost sketches refer to bc and C_{2v} complexes, the bottom-most one to two H atoms located at a bc site and an ab (anti-bonding) site on the N side of the Ga(or In)-H_{bc}-N-H_{ab} complex (also referred to as H₂ab complex). a–f) Formation energies of different As-H and N-H complexes as a function of the Fermi level. The range of the energy gap, 0.0–0.92 eV, corresponds to the estimated, partially recovered InGaAs energy gap, see the Section 3.2.

Driven by previous studies on hydrogenated $GaAs_{1-x}N_x$,^[1,4–6,19] $InAs_{1-x}N_x$,^[15] and $In_yGa_{1-y}As_{1-x}N_x$,^[20,21] as well as $In_{1-x}Ga_xN$ alloys,^[22] we investigated several complexes coming from the interactions of H atoms with host and N atoms. Such investigations concerned geometries, formation energies H_f ,^[23] formation reactions and DFT Heyd–Scuseria–Ernzerhof hybrid functional (DFT-HSE)^[24] energy gaps.

In the InGaAsN lattice, a H atom can form a charged $As-H_{bc}(+)$ or a neutral $As-H_{bc}(0)$ complex (see Figure 3), where H is located at the bc (bond-centered) site of a Ga-As (or In-As) bond that is broken and replaced by an As-H bond. Alternatively, H can form a $iH(-1)$ complex (not shown in Figure 3) where a H atom occupies an almost tetrahedral interstitial site in the lattice. Figure 3a,d shows the H_f dependence on the Fermi level (E_F) of these three

complexes, in the 4Ga-As and 4In-As environments, respectively. The H_f graphs show the stable charge state for each complex at different E_F values. The crossing point between two H_f lines defines the transition level value, $\epsilon(n/n + 1)$, that is, the E_F position where a complex changes its charge state from n to $n + 1$.^[19,23] The $As-H_{bc}(+)$ H_f line does not cross the other ones in the whole energy gap range, that is, the complex is always stable in the +1 charge state. This indicates a shallow donor behavior of H.

$H_{bc}(+)$ ions migrate in the crystal lattice attracted by the N negative charge,^[1] giving rise to exothermic reactions like, for example, $(4Ga)N + As-H_{bc}(+) \rightarrow (4Ga)N-H_{bc}(+)$, see Section S2, Supporting Information. Given the shallow donor behavior of H, this reaction is the only possible initial step for the formation of an N–H complex in the InGaAsN lattice.

Table 2. The first row of the Table reports the DFT-HSE band gap energies, E_g (eV), calculated by using the 4Ga-N (as-grown alloy) and 4In-N (annealed alloy) InGaAsN models without hydrogen. E_g values induced by the formation of N–H_{bc}(+) and C_{2v}+2 N–H complexes with the corresponding 4Ga-N and 4In-N clusters are given in the second row. For a comparison, the calculated InGaAs energy gap is 1.01 eV.

	4Ga-N	4In-N	4Ga-N	4In-N
	H _{bc} (+)	H _{bc} (+)	C _{2v} +2	C _{2v} +2
E_g (InGaAsN) [eV]	0.66	0.81	0.66	0.81
E_g (InGaAsN + H) [eV]	0.86	0.93	1.04	1.03

The N–H_{bc}(+) complex could acquire one or two free electrons to form a neutral or negatively charged complex. At variance with As–H, no geometry rearrangement is found and N–H_{bc}(0) and N–H_{bc}(–) complexes result to be the most stable neutral and negatively charged complexes, respectively. Their H_f values are reported in Figure 3b,e, together with the N–H_{bc}(+) ones, for the 4Ga-N and 4In-N clusters, respectively. H behaves as a shallow donor in both N environments.

Di-hydrogen complexes were also investigated: the C_{2v} one,^[1,25–27] see Figure 3, clearly identified in GaAs_{1–x}N_x,^[1,26,28,29] and various H₂⁺-like complexes having on-line configurations where two H atoms occupy a bc and/or an ab sites (see Figure 3 and Section S3, Supporting Information). Only the most stable H₂⁺ complex, that is, the H₂⁺ Ga(or In)–H_{bc}–N–H_{ab} complex (also referred to as H₂⁺ab complex) is shown in Figure 3. H₂⁺ complexes were recently proposed in InGaAsN.^[20,21]

In InGaAsN, given the predominance of H_{bc}(+) species, both C_{2v} and H₂⁺ complexes can initially form only in the +2 charge state and then possibly acquire free electrons and modify their geometries through H atom re-orientations. Therefore, we investigated the +2, +1, and 0 charge states of these complexes for both 4Ga-N and 4In-N clusters, see Section S3, Supporting Information. H_f values of the C_{2v} and H₂⁺ab complexes are shown in Figure 3c,f for the two N environments, respectively. In both cases, the C_{2v} complexes are stable in the +2 charge state and lower in energy than the H₂⁺ab+2 complex in the whole energy gap range. This rules out the formation of H₂⁺ complexes.

The H-induced neutralization of the effects of N was investigated by considering the DFT-HSE energy gaps calculated for the 4Ga-N (as-grown alloy) and 4In-N (annealed alloy) models without H and for the N–H_{bc}(+) and C_{2v}+2 complexes formed with the corresponding N clusters, see Table 2.

The energy gap of the 4In-N alloy model increases with respect to that of the 4Ga-N one, in agreement with the trend shown by the experimental gaps of the corresponding alloys (see Table 1). N–H_{bc}(+) complexes increase the energy gap but they do not fully recover the InGaAs gap, 1.01 eV, in the cases of both 4Ga-N and 4In-N clusters, while C_{2v}+2 complexes do, in both N environments. The homogeneous behavior of these two complexes in the two N environments gives an important indication: only different ratios between the concentrations of the two complexes in the as-grown and annealed InGaAsN could explain why H seems much more effective in neutralizing the effects of N in the as-grown material (predominantly Ga-rich N environment) than in the annealed samples (increasingly In-rich N environment).

Complex concentrations are controlled by kinetic effects related to the experimental hydrogenation conditions. Their accurate estimate is, therefore, beyond the scope of the present

study. Nevertheless, important indications can be given by the formation energies of Figure 3, which permit to estimate the concentration of each complex in thermodynamic equilibrium conditions. In InGaAsN, H_f values must be taken with respect to the bottom of the conduction band (BCB), where the E_F level is pinned by the H shallow donor behavior, see Figure 4.

As shown in Figure 4, with respect to the BCB, the H_f values of the N–H_{bc}(+) and C_{2v}+2 complexes are nearly identical for the 4Ga-N cluster, whereas they are significantly different in the 4In-N environment. From these H_f values, the estimates of the ratios between the concentrations of the two complexes (at room temperature) [N–H_{bc}(+)]/[C_{2v}+2] are much different, equal to 4×10^3 and ≈ 7 , in the cases of 4In-N clusters and 4Ga-N clusters, respectively (see Section 3.2).

Although the above estimates hold only at thermodynamic equilibrium (not reached in the present experiments), such a striking difference between the two ratios led us to assume a substantial coexistence of the two complexes in the Ga-rich N environment, replaced by a full predominance of the N–H_{bc}(+) complex in the In-rich one. These results, together with those reported in Table 2, already give a full, qualitative explanation of the experimental findings. In the as-grown InGaAsN alloy, the absence of a full energy gap recovery following H irradiation is indeed accounted for by the predominance of 4Ga-N clusters and by the ensuing coexistence of two complexes, among which only the C_{2v}+2 fully neutralizes the effects of N. In the annealed alloys, the increasing preponderance of 4In-N clusters hinders the formation of the complex most effective for N passivation, thus accounting for the observed reduction in hydrogen's ability to cause the energy gap recovery. The above estimates of the N–H_{bc}(+) and C_{2v}+2 concentrations can be used for a refinement of the results of Table 2, leading to a satisfactory agreement with the experiment, see Section S4, Supporting Information. Here, we focus on a puzzling question posed by the above results: why do N–H complexes showing such similar properties form in much different concentration ratios when the cation-N environment changes? Our answer implies a change of perspective. Let us consider the N–H_{bc}(+) and C_{2v}+2 complexes forming in InGaAsN, either in the 4Ga-N or in the 4In-N environment, as units inserted in the host InGaAs matrix. Then, let us compare their formation with that of the same units in the GaAsN and InAsN alloys, where they necessarily form in the 4Ga-N and 4In-N environments and are inserted in the GaAs and InAs matrices, respectively. What is the advantage of such a comparison? For the N–H_{bc}(+) complex in InGaAsN, the breaking of a Ga–N or an In–N bond and its replacement by a N–H bond induces an increase of the cation–N distance of more than a 60%, see Figure 3. This implies a significant local strain around the N atom, which gets even higher in the case of the C_{2v}+2 complex, where the number of bonds broken and replaced amounts to 2.^[30] The energy balance governing the formation of either complex consists of two contributions: the balance of chemical bond energies and the cost in energy due to the local strain. When investigating a given complex, for example, the C_{2v}+2 in the 4In-N (4Ga-N) environment, the bond energy balance is almost identical in InGaAsN and InAsN (GaAsN), as it corresponds to the dissociation and formation of almost identical chemical bonds (see Section S2, Supporting Information). Therefore, most of the difference in the energetics of the complexes may be ascribed to the difference in the strain energy.

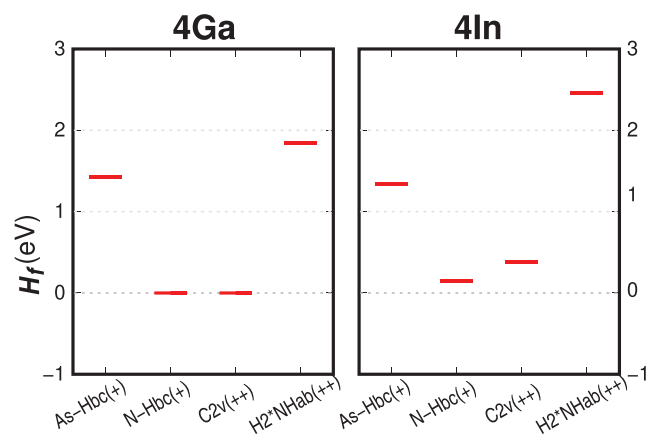


Figure 4. Formation energies H_f of the most important As-H and N-H charged complexes, taken from Figure 3 with respect to the bottom of the conduction band (BCB), are reported as red lines in the figure.

In InGaAsN and InAsN (GaAsN) alloys, the local strain induced by the formation of a N-H complex in the 4In-N (4Ga-N) environment can be related to the volume expansion of the 4In (4Ga) tetrahedron surrounding the N atom, see Figure 3. In fact, for example, in InAsN, the volumes of the N-H_{bc}(+) and C_{2v}+2 N-tetrahedra increase by 55% and 126% with respect to that of an isolated N atom, respectively. In InGaAsN, the corresponding volume expansions amount to 47% and 102%, respectively. The two complexes show smaller volume expansions in InGaAsN because the N-tetrahedron expands against a host InGaAs matrix which has a smaller unit cell and a larger bulk modulus (i.e., a larger stiffness) than the host InAs matrix of InAsN (see Section S5, Supporting Information). Thus, both the N-H_{bc}(+) and the C_{2v}+2 complexes have to pay a higher strain energy cost when forming in the stiffer host matrix, as testified by the decrease of the corresponding tetrahedron volume expansions. Of course, the formation of the C_{2v}+2 complex, which requires a larger tetrahedron expansion than N-H_{bc}(+), is more severely affected by the stiffness of the host matrix. This critical, discriminating effect on the formation of the two complexes can be quantified by estimating the ratios between the volume expansions of the C_{2v}+2 and N-H_{bc}(+) tetrahedra in InGaAsN and InAsN, 2.17 and 2.29, respectively. These values confirm the larger hindrance influencing the C_{2v}+2 formation (with respect to N-H_{bc}(+)) in InGaAsN. Albeit small, their difference is a significant one. In fact, let us consider the 4Ga-N environment and examine the formation of the same two complexes in InGaAsN and in GaAsN. Now, the InGaAs matrix is the one with a larger unit cell and a smaller bulk modulus with respect to GaAs (see Section S5, Supporting Information); therefore, there is a lower opposition to the formation of these complexes in InGaAsN than in GaAsN. In the two materials, indeed, the volumes of the C_{2v}+2 N-tetrahedron increase by 129% and 124%, while those of the N-H_{bc}(+) N-tetrahedron are 55% and 53% higher, respectively. At variance with the previous case, the larger increase occurs now in InGaAsN. Moreover, the ratio between the volume expansions of the two complexes is equal to 2.34 in both alloys, showing that the different opposition to their formation, found in the InGaAsN-InAsN comparison, has disappeared. Accordingly, when in a 4Ga-N

environment in InGaAsN, the C^{2v}+2 and the N-H_{bc}(+) complexes form in comparable concentrations, as suggested by the H_f values in Figure 4.

The above considerations (further results in Section S5, Supporting Information) lead to the remarkable conclusion that for N-H complexes forming in the 4In-N environment, and only in this environment, the InGaAsN host matrix exerts a selective action favoring the formation of the N-H_{bc}(+) complex (less effective in neutralizing the effects of N), thus explaining thoroughly the occurrence of different N-H complex concentrations in the two different cation-N environments. This result also fully accounts for the experimental observation that annealed InGaAsN samples (predominant In-rich N environment) are significantly less sensitive to H irradiation than the nonannealed material (predominant Ga-rich environment).

The present results reveal, therefore, the existence of a novel physical phenomenon, where a major role is played by the matrix surrounding the N-H complex. They also clarify its origin, which is traced back to the two-component nature of the InGaAs alloy, more specifically, to the different mechanical properties of its GaAs and InAs components. This important finding could open further routes for the development of new protocols for the tuning of the material properties, which can be based on an integrated matrix/defect engineering approach, with immediate impact on both the material design and the realization of quantum confining structures. About the former feature, the proposed model is not limited to III-V-N alloys, under the (very reasonable) assumption that it may be generalized to alloys presenting parallel features, for example, N doped SiC, SiC:N, where C:N and Si:N play the role of GaAsN and InAsN, respectively.^[31–33] Regarding the quantum structures, for example, as-grown InGaAsN could be locally annealed by exposure to a focused laser beam. Upon hydrogenation these annealed regions would be lower-energy gap areas, wherein carriers could be laterally confined. In principle, the size of these carrier-confining potentials could be pushed to the nanoscale by applying the subwavelength light-focusing techniques recently applied to the fabrication of site-controlled GaAsN:H/GaAsN quantum dots,^[10,11] thus demonstrating the potential of the novel approach proposed here.

3. Experimental Section

Experimental Details: Two types of In_yGa_{1-y}As_{1-x}N_x/GaAs QW samples grown by metalorganic vapor phase epitaxy on a GaAs substrate were investigated. The first type consisted in a double QW structure,^[34] with the In_yGa_{1-y}As_{1-x}N_x QW on top of the In_yGa_{1-y}As QW. The deposition sequence is as follows. First, a thick (200 nm) GaAs buffer was grown at 590 °C. After a growth interruption to decrease the temperature down to 520 °C, the 5.6 nm-thick In_{0.25}Ga_{0.75}As reference QW was deposited and the temperature was brought back to 590 °C. During this process the arsine flux was kept high (As/III = 100). A 50 nm GaAs layer was then deposited before interrupting again the growth to lower the reactor temperature. The In_{0.25}Ga_{0.75}As_{1-x}N_x QW (thickness equal to 5.6 nm as the reference QW) was deposited using a 2-step growth method intended to prevent the N accumulation at the first growth interface. The InGaAsN was deposited in two successive layers: 1.5 nm at 520 °C with moderate DMHy flux (26 ccm) followed by 4.1 nm with higher flux (190 ccm). The As/III = 8 ratio was kept low during the N-containing QW

deposition, and a similar arsine flux was used during the last minutes of the preceding growth interruption. The N concentration was estimated by PL to be ≈ 0.015 . The temperature was finally increased to 590 °C to deposit a 100 nm GaAs cap.

The second type of sample consisted in a single $\text{In}_y\text{Ga}_{1-y}\text{As}_{1-x}\text{N}_x/\text{GaAs}$ QW. The deposition sequence is as follows. First, a thick (250 nm) GaAs buffer was grown at 650 °C. After a growth interruption to decrease the temperature down to 525 °C, a 5 nm thick $\text{In}_{0.21}\text{Ga}_{0.79}\text{As}_{0.97}\text{N}_{0.03}$ QW was deposited. The As/Ga ratio was kept at 7 during the QW growth. The UDMHy/TBAs ratio for the QW growth was 67. After the QW growth, a 90 nm thick GaAs cap was grown also at 525 °C. Subsequently the sample was annealed for 5 min at 725 °C under TBAs stabilization. The sample was also annealed ex situ in an N_2 environment under atmospheric pressure with a GaAs proximity cap. The heating ramp was in the range of 7 K s^{-1} . Three annealing conditions were employed: 600 °C for 10 s, 650 °C for 30 s, and 750 °C for 10 s. As reported previously,^[16] these conditions modified the atomic rearrangement in the InGaAsN lattice without changing the average composition of the QW (namely, without causing In/Ga diffusion in the barrier/QW).

Finally, the samples were proton- or deuteron-irradiated at $T_1 = 300$ °C by a Kaufman source (100 eV per ion beam energy) with typical ion impinging current density of few tens of $\mu\text{A cm}^{-2}$.

PL measurements were recorded at room temperature, in order to avoid contribution from the localized states that typically dominate the spectra at cryogenic temperatures ($T < 150$ K).^[35] This allowed to reliably determine the effective band gap energy of the QW, which was assumed to coincide with the PL peak energy. PL was excited by a 532 nm laser, spectrally analyzed by a 0.75 m focal length monochromator and detected by a liquid nitrogen-cooled InGaAs linear array.

SIMS measurements were performed on the double QW sample treated with deuterium (D is equivalent to H in terms of its interaction with N, but SIMS measurements are experimentally more sensitive to the heavier isotope). A $E_{\text{Cs}}=1$ keV Cs^+ primary beam at oblique incidence (55°) was used in a CAMECA Sc-Ultra mass spectrometer where $^2\text{D}^-$, $^{14}\text{N}^-$, $^{70}\text{Ga}^-$, and $^{115}\text{In}^-$ negative secondary ions were collected with a depth resolution of 2–3 nm decade $^{-1}$. Other impact energies and incidence angles versus surface normal were tested in order to identify the best analytical conditions for this class of samples. 1 keV at 55° were the best conditions for signal to noise ratio and for depth resolution. The sputtering time was converted to an in-depth scale by measuring the obtained crater depths by a mechanical stylus profilometer.

Theoretical Methods: DFT-HSE with the range-separated HSE06 hybrid functional,^[24,36] as implemented with plane wave basis sets in the QUANTUM-ESPRESSO^[37,38] suite of programs was used here for the investigation of the equilibrium structures and electronic properties of the InGaAsN alloy and of the complexes formed by atomic H with N and with the host atoms in this alloy, as well as for understanding the effects of the complex formation on the host energy gap. In this regard, as performed in a previous study,^[15] in all of the systems investigated here the energy gap values were estimated by the Kohn–Sham (KS) hybrid functional eigenvalues. The properties of hydrogenated and pristine InGaAsN and InGaAs alloys were investigated by using 64-atom supercells simulating $\text{In}_{0.20}\text{Ga}_{0.80}\text{As}_{0.97}\text{N}_{0.03}$ and $\text{In}_{0.20}\text{Ga}_{0.80}\text{As}$ alloys close in stoichiometry to the measured samples, where the Ga and In cations were randomly distributed (see Section S1, Supporting Information). 64-atom supercells assured a satisfactory convergence in the case of GaAs and GaAsN.^[15] Thus, they were used here for the investigation of the present GaAs-rich alloys. Nuclei and core electrons were substituted by optimized norm-conserving Vanderbilt’s pseudopotentials.^[39] Explicit valence pseudo-wavefunctions were 2s and 2p for N; 3s and 3p for As; 3d, 4s and 4p for Ga; 4d, 5s and 5p for In. The plane wave and density cutoffs were 80 and 320 Ry, respectively. The short-range part of the hybrid exchange functional is defined as a linear combination of exact Hartree–Fock exchange and GGA exchange

$$E_x^{\text{hybr}} = \alpha E_x^{\text{Fock}} + (1 - \alpha) E_x^{\text{CGA}} \quad (1)$$

In a previous study of N–H complexes in the GaAsN and InAsN alloys,^[15] the coefficient α was chosen in order to best describe the KS band gap of InAs, given the rather small energy gap of this semiconductor: $\alpha = 0.32$ was the best choice. Errors induced in the InAs and GaAs KS band gaps were around 0.2% and 7%, respectively. Errors on the InAsN and GaAsN energy gaps amounted to 16% and 17%, respectively. In order to perform a consistent comparison between previous and present results, the same value for the α parameter was used here. This led to errors of 29% and 20%, with respect to the experimental data, when the as-grown and annealed InGaAsN alloys were simulated by $\text{In}_{0.20}\text{Ga}_{0.80}\text{As}_{0.97}\text{N}_{0.03}$ models containing only 4Ga–N and 4In–N clusters, respectively. Notwithstanding, present results gave reliable indications on the H effects on the energy gap. In fact, first, the calculated $\text{In}_{0.20}\text{Ga}_{0.80}\text{As}$ energy gap, 1.01 eV, was affected by a comparable error of about 23% with respect to the estimated value of 1.32 eV corresponding to the vertical dashed line labeled as ref. in Figure 2b of the main text. Second, N–H complexes raising the energy gap to its theoretical value (1.01 eV) guaranteed a full passivation of the N effects.

Given the heavy computational demand of hybrid functional simulations, geometry optimizations were performed sampling the Brillouin zone at the Γ point. Total energies and electronic eigenvalues were obtained by single-point calculations on a $2 \times 2 \times 2$ k-point mesh including the Γ point.

In the present study, a further fundamental quantity was the formation energy of a complex formed by H with the N atom and/or the host atoms, H_f . For instance, in the case of a N–H complex in the q charge state and containing n H atoms, H_f is given by the expression (see, e.g., Ref. [23, 40], and references therein)

$$H_f[N - nH](q) = E[N - nH](q) - E[N] - n\mu_H + q(E_F + \epsilon_{\text{VB}}) \quad (2)$$

where $E[N - nH](q)$ and $E[N]$ are the total energies of the supercells containing the complex in a charge state q , and, respectively, the nitride alloy without H. The third term keeps into account the addition to the system of n hydrogen atoms ($n > 0$), considered at a chemical potential μ_H . Here, μ_H corresponds to half of the total energy of a H_2 molecule in vacuum. Electrons were given to or taken from (in agreement with the q value) a reservoir, whose chemical potential was the Fermi level E_F , referred to the valence band maximum, ϵ_{VB} . Thus, it is seen from Equation (2) that the formation energies H_f follow the Fermi level E_F as straight lines, whose slope is given by the complex charge, q , as shown in Figure 3.

Formation energies as defined in Equation (2) may be used to determine the charge states of a complex in the system as a function of the Fermi level of the electron reservoir. Equating formation energies of the N- n H complex in the charge states q and q' gives the transition level

$$\epsilon(q/q') = \frac{E[N - nH](q') - E[N - nH](q)}{q - q'} - \epsilon_{\text{VB}} \quad (3)$$

that is the Fermi level value at which the complex passes from charge q to charge q' .^[23]

The formation energy of a N–H complex had to be computed for values of E_F within a given energy gap range. When H fully passivates the effects of N (e.g., in the case of GaAsN), the energy gap range was that of the material without N (i.e., GaAs). In InGaAsN, it had to be taken into account that H recovered only a 91% of the InGaAs gap, as shown by the experimental data reported in Figure 1, where 1.115 and 1.220 eV energy gaps were measured for the hydrogenated InGaAsN QW and for the pristine InGaAs QW, respectively. According to the simulations, the theoretical estimate of the InGaAs gap is equal to 1.01 eV. Thus, the maximum value reachable by the energy gap of the hydrogenated InGaAsN is equal to 0.92 eV, as reported in Figures 3 and 4.

Formation energies also permitted to estimate the concentration of an X complex in thermodynamic equilibrium conditions, $[X]$, which is given by the expression^[23]

$$[X] = N_{\text{sites}} N_{\text{config}} \exp(-H_f^X/kT), \quad (4)$$

where N_{sites} is the number of sites in the lattice per unit volume where the complex can be incorporated, N_{config} is the number of equivalent configurations in which the complex can be formed, k is the Boltzmann's constant, and T is the temperature.

Here, the need is to estimate the ratio of the complex concentrations, $[N-H_{bc}(+)]/[C_{2v}+2]$ or $[X1]/[X2]$, that is:

$$[X1]/[X2] = R_{\text{config}} \exp\left[\frac{(H_f^{X2} - H_f^{X1})}{kT}\right] \quad (5)$$

where it has been taken into account that N_{sites} has the same value for both complexes and the ratio $N_{\text{config}}(X1)/N_{\text{config}}(X2)$, R_{config} , is equal to 0.67.

Supporting Information

Supporting Information is available from the Wiley Online Library or from the author.

Acknowledgements

The authors would like to acknowledge Dr. Alok Rudra, from Ecole Polytechnique Fédérale de Lausanne (EPFL), Switzerland, for his precious support to the logistics of the MOVPE facility in the Laboratory of Physics of Nanostructures.

Open access funding provided by Consiglio Nazionale delle Ricerche within the CRUI-CARE Agreement.

Conflict of Interest

The authors declare no conflict of interest.

Data Availability Statement

Research data are not shared.

Keywords

density functional theory, hydrogen doping, InGaAsN alloys

Received: September 6, 2021

Revised: October 4, 2021

Published online:

- [1] *Hydrogenated Dilute Nitride Semiconductors* (Ed: G. Ciatto), Pan Stanford, Singapore **2015**.
- [2] A. Albo, D. Fekete, G. Bahir, *Infrared Phys. Technol.* **2019**, 96, 68.
- [3] M. Felici, A. Polimeni, G. Salviati, L. Lazzarini, N. Armani, F. Masia, M. Capizzi, F. Martelli, M. Lazzarino, G. Bais, M. Piccin, S. Rubini, A. Franciosi, *Adv. Mater.* **2006**, 18, 1993.
- [4] Y.-S. Kim, K. J. Chang, *Phys. Rev. B* **2002**, 66, 073313.
- [5] A. Janotti, S. B. Zhang, S.-H. Wei, C. G. Van de Walle, *Phys. Rev. Lett.* **2002**, 89, 086403.
- [6] A. Amore Bonapasta, F. Filippone, P. Giannozzi, M. Capizzi, A. Polimeni, *Phys. Rev. Lett.* **2002**, 89, 216401.

- [7] E. P. O'Reilly, A. Lindsay, P. J. Klar, A. Polimeni, M. Capizzi, *Semicond. Sci. Technol.* **2009**, 24, 033001.
- [8] P. J. Klar, H. Grüning, M. Güngerich, W. Heimbrodt, J. Koch, T. Torunski, W. Stolz, A. Polimeni, M. Capizzi, *Phys. Rev. B* **2003**, 67, 121206(R).
- [9] M. Felici, G. Pettinari, F. Biccari, A. Boschetti, S. Younis, S. Birindelli, M. Gurioli, A. Vinattieri, A. Gerardino, L. Businaro, M. Hopkinson, S. Rubini, M. Capizzi, A. Polimeni, *Phys. Rev. B* **2020**, 101, 205403.
- [10] F. Biccari, A. Boschetti, G. Pettinari, F. La China, M. Gurioli, F. Intonti, A. Vinattieri, M. Sharma, M. Capizzi, A. Gerardino, L. Businaro, M. Hopkinson, A. Polimeni, M. Felici, *Adv. Mater.* **2018**, 30, 1705450.
- [11] A. Ristori, T. Hamilton, D. Toliopoulos, M. Felici, G. Pettinari, S. Sanguinetti, M. Gurioli, H. Mohseni, F. Biccari, *Adv. Quantum Technol.* **2021**, 4, 2100045.
- [12] Y. Park, M. J. Cich, R. Zhao, P. Specht, H. Feick, E. R. Weber, *Phys. B: Condens. Matter* **2001**, 308–310, 98.
- [13] S. Birindelli, M. Kesaria, D. Giubertoni, G. Pettinari, A. V. Velichko, Q. D. Zhuang, A. Krier, A. Patané, A. Polimeni, M. Capizzi, *Semicond. Sci. Technol.* **2015**, 30, 105030.
- [14] A. V. Velichko, A. Patané, M. Capizzi, I. C. Sandall, D. Giubertoni, O. Makarovskiy, A. Polimeni, A. Krier, Q. Zhuang, C. H. Tan, *Appl. Phys. Lett.* **2015**, 106, 022111.
- [15] F. Filippone, G. Mattioli, A. Polimeni, M. Felici, A. Amore Bonapasta, *J. Phys. Chem. C* **2020**, 124, 19240.
- [16] C. Peng, H. Liu, J. Konttinen, M. Pessa, *J. Cryst. Growth* **2005**, 278, 259.
- [17] P. J. Klar, H. Grüning, J. Koch, S. Schäfer, K. Volz, W. Stolz, W. Heimbrodt, A. M. K. Saadi, A. Lindsay, E. P. O'Reilly, *Phys. Rev. B* **2001**, 64, 121203.
- [18] S. Kurtz, J. Webb, L. Gedvilas, D. Friedman, J. Geisz, J. Olson, R. King, D. Joslin, N. Karam, *Appl. Phys. Lett.* **2001**, 78, 748.
- [19] C. Van de Walle, J. Neugebauer, *Nature* **2003**, 423, 626.
- [20] T. Mou, S. Li, C. R. Brown, V. R. Whiteside, K. Hossain, M. Al Khalfoui, M. Leroux, I. R. Sellers, B. Wang, *ACS Appl. Electron. Mater.* **2019**, 1, 461.
- [21] C. R. Brown, N. J. Estes, V. R. Whiteside, B. Wang, K. Hossain, T. D. Golding, M. Leroux, M. Al Khalfoui, J. G. Tischler, C. T. Ellis, E. R. Glaser, I. R. Sellers, *RSC Adv.* **2017**, 7, 25353.
- [22] G. Pettinari, F. Filippone, A. Polimeni, G. Mattioli, A. Patané, V. Lebedev, M. Capizzi, A. Amore Bonapasta, *Adv. Funct. Mater.* **2015**, 25, 5353.
- [23] C. G. Van de Walle, J. Neugebauer, *J. Appl. Phys.* **2004**, 95, 3851.
- [24] J. Heyd, G. E. Scuseria, M. Ernzerhof, *J. Chem. Phys.* **2006**, 124, 219906.
- [25] A. Amore Bonapasta, F. Filippone, P. Giannozzi, *Phys. Rev. B* **2003**, 68, 115202.
- [26] W. B. Fowler, K. R. Martin, K. Washer, M. Stavola, *Phys. Rev. B* **2005**, 72, 035208.
- [27] M.-H. Du, S. Limpijumnong, S. B. Zhang, *Phys. Rev. B* **2005**, 72, 073202.
- [28] S. Kleekajai, F. Jiang, K. Colon, M. Stavola, W. B. Fowler, K. R. Martin, A. Polimeni, M. Capizzi, Y. G. Hong, H. P. Xin, C. W. Tu, G. Bais, S. Rubini, F. Martelli, *Phys. Rev. B* **2008**, 77, 085213.
- [29] L. Wen, F. Bekisli, M. Stavola, W. B. Fowler, R. Trotta, A. Polimeni, M. Capizzi, S. Rubini, F. Martelli, *Phys. Rev. B* **2010**, 81, 233201.
- [30] A. Polimeni, G. Ciatto, L. Ortega, F. Jiang, F. Boscherini, F. Filippone, A. Amore Bonapasta, M. Stavola, M. Capizzi, *Phys. Rev. B* **2003**, 68, 085204.
- [31] M. N. R. Ashfold, J. P. Goss, B. L. Green, P. W. May, M. E. Newton, C. V. Peaker, *Chem. Rev.* **2020**, 120, 5745.
- [32] F. Casola, T. van der Sar, A. Yacoby, *Nat. Rev. Mater.* **2018**, 3, 17088.
- [33] J. Y. Tsao, S. Chowdhury, M. A. Hollis, D. Jena, N. M. Johnson, K. A. Jones, R. J. Kaplar, S. Rajan, C. G. Van de Walle, E. Bellotti, C. L. Chua, R. Collazo, M. E. Coltrin, J. A. Cooper, K. R. Evans,

- S. Graham, T. A. Grotjohn, E. R. Heller, M. Higashiwaki, M. S. Islam, P. W. Juodawlkis, M. A. Khan, A. D. Koehler, J. H. Leach, U. K. Mishra, R. J. Nemanich, R. C. N. Pilawa-Podgurski, J. B. Shealy, Z. Sitar, M. J. Tadjer, et al., *Adv. Electron. Mater.* **2018**, 4, 1600501.
- [34] D. Fekete, R. Carron, P. Gallo, B. Dwir, A. Rudra, E. Kapon, *Appl. Phys. Lett.* **2011**, 99, 072116.
- [35] A. Polimeni, M. Capizzi, M. Geddo, M. Fischer, M. Reinhardt, A. Forchel, *Appl. Phys. Lett.* **2000**, 77, 2870.
- [36] J. Heyd, G. E. Scuseria, M. Ernzerhof, *J. Chem. Phys.* **2003**, 118, 8207.
- [37] P. Giannozzi, O. Andreussi, T. Brumme, O. Bunau, M. B. Nardelli, M. Calandra, R. Car, C. Cavazzoni, D. Ceresoli, M. Cococcioni, N. Colonna, I. Carnimeo, A. D. Corso, S. de Gironcoli, P. Delugas, R. A. DiStasio, A. Ferretti, A. Floris, G. Fratesi, G. Fugallo, R. Gebauer, U. Gerstmann, F. Giustino, T. Gorni, J. Jia, M. Kawamura, H.-Y. Ko, A. Kokalj, E. Küçükbenli, M. Lazzeri, et al., *J. Phys.: Condens. Matter* **2017**, 29, 465901.
- [38] P. Giannozzi, S. Baroni, N. Bonini, M. Calandra, R. Car, C. Cavazzoni, D. Ceresoli, G. L. Chiarotti, M. Cococcioni, I. Dabo, A. D. Corso, S. de Gironcoli, S. Fabris, G. Fratesi, R. Gebauer, U. Gerstmann, C. Gougoussis, A. Kokalj, M. Lazzeri, L. Martin-Samos, N. Marzari, F. Mauri, R. Mazzarello, S. Paolini, A. Pasquarello, L. Paulatto, C. Sbraccia, S. Scandolo, G. Sclauzero, A. P. Seitsonen, et al., *J. Phys.: Condens. Matter* **2009**, 21, 395502.
- [39] D. R. Hamann, *Phys. Rev. B* **2013**, 88, 085117.
- [40] W. Chen, A. Pasquarello, *J. Phys.: Condens. Matter* **2015**, 27, 133202.